Inorganic Chemistry

Article

pubs.acs.org/IC

$Li_2Ni_{0.5}Mn_{0.5}SnO_4/C$: A Novel Hybrid Composite Electrode for High Rate Applications

Mani Vellaisamy and Kalaiselvi Nallathamby*

CSIR-Central Electrochemical Research Institute, Karaikudi 630 006, Tamilnadu, India

Supporting Information

ABSTRACT: A novel $Li_2Ni_{0.5}Mn_{0.5}SnO_4/C$ composite electrode, existing as a hybrid consisting of monoclinic Li_2SnO_3 and layered $LiNi_{0.5}Mn_{0.5}O_2$, has been identified and validated for high capacity and high rate lithium battery applications. Of the components, $LiNi_{0.5}Mn_{0.5}O_2$ upon discharge forms the corresponding dilithium oxide, viz., $Li_2Ni_{0.5}Mn_{0.5}O_2$, and facilitates the progressive electrochemical performance of the composite electrode. Similarly, Li_2SnO_3 upon discharge forms Li_2O and SnO_2, wherein the unacceptable volume expansion related issues of SnO_2 are addressed by the buffering activity of Li_2O phase. A combination of alloying/dealloying, conversion, and redox mechanism is responsible for the excellent electrochemical behavior of $Li_2Ni_{0.5}Mn_{0.5}SnO_4/C$ electrode. With this newer formulation of dilithium stannate composite, a superior capacity of >3000 mAh g^{-1} at 100 mA g^{-1} current density has been demonstrated. The study opens up a newer gateway for the entry of $Li_2SnO_3{\cdot}LiM_1M_2O_2$ hybrid formulations for exploitation up to 1 A g^{-1} rate, thus ensuring the sustainable development of potential electrode materials for high rate applications.

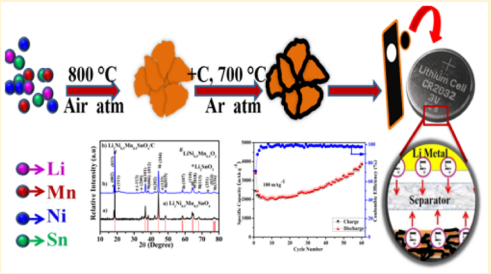

1. INTRODUCTION

Among the three types of lithium battery electrodes, viz., insertion compounds,[1,2] active metal facilitating compounds,[3,4] and Li_2O + catalytic transition metal composite forming derivatives,[5,6] the last category electrodes exhibit closer resemblance with that of hybrid cathodes containing electrochemically active and inactive components together. For example, layered $Li_{1.5}Mn_{0.75}Ni_{0.25}O_{2.5}$ cathode[7] could be best represented as $0.5Li_2MnO_3{\cdot}0.5LiNi_{0.5}Mn_{0.5}O_2$ wherein the Mn^{4+} ions (electrochemically inactive) improve the stability and enhance the overall electrochemical performance. Quite similar to such Li_2MnO_3 stabilized electrode materials, recently a combination of electrochemically inactive Li_2O and electrochemically active monoclinic Li_2SnO_3 phase and cubic Mn_2SnO_4 phase components, coexisting in Li_2MnSnO_4/C composite anode, has been reported.[8] Herein, a combination of conversion, displacement, and alloying/dealloying mechanism has been found to be responsible for the improved electrochemical behavior, compared with that of the conventional graphite.[9]

Buffering of anticipated volume expansion related issues, formation and decomposition of $Li_{4.4}Sn$ alloy, and the redox behavior associated with the $Mn^{2+} \leftrightarrow Mn^0$ couple respectively due to the presence of Li_2O, Li_2SnO_3, and Mn_2SnO_4 contribute in a major way to consider the newly identified Li_2MnSnO_4/C as a potential anode for rechargeable lithium battery applications.[8]

In this case, it is important to note that the exciting improvement realized with respect to the electrochemical behavior is found selectively with the Li_2MnSnO_4/C composite, because pristine Li_2MnSnO_4, despite its existence as a stable and single phase compound, has been found to suffer from inferior electrochemical properties, when deployed as a lithium intercalating anode material. Such an observation triggers a few queries: (a) Do all $Li_xM_ySnO_4$ electrodes require the formation of corresponding carbon composite to obtain the desired and hybrid combination of suitable components to address the capacity fade related issues? (b) Can carbon addition solely address the inferior electrochemical performance of $Li_xM_ySnO_4$ family electrodes with inherent poor electronic conductivity by way of improving the conductivity and thereby increasing the lithium transport kinetics, which is responsible for facile intercalation/de-intercalation of lithium ions? (c) To what extent are the existence and recombination of hybrid components important, especially in view of the electrochemical behavior of $Li_xM_ySnO_4$ electrode? In an attempt to answer the said queries, a carefully coined formulation of $Li_2Ni_{0.5}Mn_{0.5}SnO_4$ compound has been investigated for the study. Herein, partial replacement of Mn^{2+} with Ni^{2+} has been considered with a view to understand whether the select dilithium stannate could perform as a potential anode similar to those of the $Li_2Ni_{0.5}Mn_{0.5}O_2$ type of dilithium oxides, because dilithium oxides, which are reported to be obtained from the corresponding monolithium oxide ($LiNi_{0.5}Mn_{0.5}O_2$) well below 2.0 V, are capable of demonstrating themselves as lithium intercalating anode materials.[10]

In other words, the choice of the title compound was based on the intriguing query raised in line with the anode behavior of dilithium oxides (obtained during the discharge of layered

Received: June 2, 2015
Published: August 7, 2015

DOI: 10.1021/acs.inorgchem.5b01246
Inorg. Chem. 2015, 54, 8590−8597

ABO_2 oxides of known type), "can it be extended to dilithium stannates also" to form the desired dilithium oxides upon discharge? To our surprise, the select $Li_2Ni_{0.5}Mn_{0.5}SnO_4$ compound, especially when prepared in the presence of excess lithium and furnace heated in open atmosphere, leads to the formation of preferred combination of hybrid structures, viz., monoclinic Li_2SnO_3 and layered $LiNi_{0.5}Mn_{0.5}O_2$, and exhibits excellent electrochemical behavior via formation of $Li_2Ni_{0.5}Mn_{0.5}O_2$. Similarly, the role of hybrid components in combating the undesirable capacity fade of $Li_2Ni_{0.5}Mn_{0.5}SnO_4$/C anode upon extended cycling and the effect of added carbon in improving the capacity of anode material by increasing the electronic conductivity to a desired level are better understood and demonstrated through the current study. A preoptimized concentration of 10 wt % super P carbon has been added to prepare $Li_2Ni_{0.5}Mn_{0.5}SnO_4$/C composite, and the superiority of thus obtained composite in improving the electrochemical performance of pristine $Li_2Ni_{0.5}Mn_{0.5}SnO_4$ compound has been discussed in detail.

A simple sol−gel method has been used to prepare $Li_2Ni_{0.5}Mn_{0.5}SnO_4$ compound and the corresponding composite by mechanothermal approach. The study leads to a new direction of understanding that dilithium stannates in their duly modified composite form could be exploited as potential anodes, similar to those of dilithium oxides. Hence, the significant leads of the current study open up a newer gateway for the entry of series of $Li_2M_1M_2SnO_4$/C composite electrodes as novel and better performing futuristic anodes for lithium ion batteries.

2. EXPERIMENTAL SECTION

2.1. Material Synthesis. $Li_2Ni_{0.5}Mn_{0.5}SnO_4$ sample was prepared by sol−gel method. Stoichiometric ratios of reactants, viz., CH_3COOLi (Alfa Aesar), $Mn(CH_3COO)_2$ (Alfa Aesar), $Ni(CH_3COO)_2$, and tin(IV) isopropoxide (Alfa Aesar), were dissolved in deionized water in which citric acid was added as complexing agent to form a gel. The solution was heated to 85 °C under vigorous stirring to obtain a gel. The as formed gel was heat treated overnight at 150 °C in a hot air oven to decompose the organic compounds and furnace heated to 300 °C for 5 h at a heating rate of 1 °C/min. The powder thus obtained was further heated to 800 °C for 3 h with intermittent grinding to obtain $Li_2Ni_{0.5}Mn_{0.5}SnO_4$ compound. To prepare $Li_2Ni_{0.5}Mn_{0.5}SnO_4$/C composite with conductive carbon, 10 wt % of super P carbon was added to the synthesized powder and ball milled (250 rpm) for 5 h. To ensure perfect adherence of added carbon on the surface of $Li_2Ni_{0.5}Mn_{0.5}SnO_4$ particles, the mixture was heated to 700 °C for 2 h in Ar atmosphere, and the same has been named as $Li_2Ni_{0.5}Mn_{0.5}SnO_4$/C composite. Herein, the rate of heating was maintained at 1 °C/min to avoid agglomeration and surface cracking of the formed particles.

2.2. Electrode Preparation and Coin Cell Assembly. The electrode was prepared from a combination of 70 wt % active composite material with 20 wt % super P carbon and 10 wt % polyvinylidene difluoride (PVdF) binder. The PVdF binder was dissolved in *N*-methylpyrrolidone, and a mixture of premixed active composite material with super P carbon has been added to the solution to get a homogeneous slurry. The slurry was coated on a Cu foil (current collector), dried under vacuum at 80 °C for 12 h, and pressed with 3 ton pressure. Such a hot roll pressed electrode was cut into a circular shape (14 mm), and the electrodes typically had an active material content of 8−10 mg. The electrode was further dried under vacuum at 80 °C for 30 min prior to the assembling of cells in an argon filled glovebox. Electrochemical characterization was carried out on freshly fabricated 2032 coin cells consisting of $Li_2Ni_{0.5}Mn_{0.5}SnO_4$/C anode vs Li^+/Li and a nonaqueous electrolyte containing 1 M $LiPF_6$ (dissolved in 1:1 v/v EC:DMC) using Celgard as a separator.

2.3. Physical and Electrochemical Characterization. Phase characterization was done by powder X-ray diffraction technique on a PANalytical X'Pert PRO X-ray diffractometer using Ni-filtered Cu Kα radiation. Surface morphology, particle size, and carbon coating of synthesized active material were investigated using Gemini field emission scanning electron microscopy (FE-SEM) and Tecnai 20 G2 (FEI make) transmission electron microscopy (TEM). HR-TEM images were recorded with a Jeol Jem 2100 TEM analyzer. X-ray photoelectron spectra (XPS) were obtained using a MULTILAB 2000 base system with an excitation source of Mg Kα radiation. TGA analysis was performed using TA Instruments SDT Q600 thermogravimetric analyzer. Nitrogen sorption analysis was carried out using a NOVA 3200e surface area and pore size analyzer. The pore size distribution plot was recorded based on the Barrett−Joyner−Halenda (BJH) model. Electrochemical studies were carried out using a VMP3 (Bio-Logic) electrochemical workstation and an ARBIN charge−discharge cycle life tester.

3. RESULTS AND DISCUSSION

The powder X-ray diffraction pattern (XRD) of $Li_2Ni_{0.5}Mn_{0.5}SnO_4$/C composite is shown in Figure 1; since

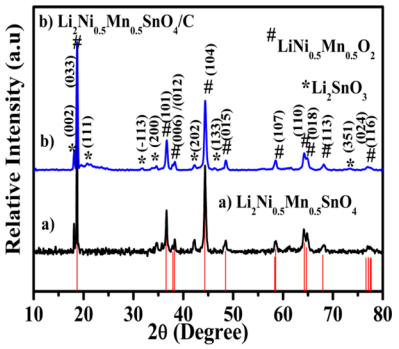

Figure 1. Powder X-ray diffraction pattern of pristine and $Li_2Ni_{0.5}Mn_{0.5}SnO_4$/C synthesized at 800 °C.

the title compound falls under the category of newly identified formulation, no JCPDS pattern is available for comparison. However, upon careful investigation using search match analysis, it is found that the target compound, viz., $Li_2Ni_{0.5}Mn_{0.5}SnO_4$, especially when prepared with excess lithium concentration (chosen intentionally to offset the anticipated lithium loss at high temperature synthesis condition) and calcined in the furnace, exists in the form of a hybrid, consisting of layered rhombohedral $LiNi_{0.5}Mn_{0.5}O_2$ and monoclinic Li_2SnO_3, according to the following equation:

$$Li_2Ni_{0.5}Mn_{0.5}SnO_4 + 3Li + O_2 \rightarrow LiNi_{0.5}Mn_{0.5}O_2 + Li_2SnO_3 + Li_2O \quad (1)$$

The sharp reflection peaks indicate the formation of a highly crystallized phase of the formed product. While a majority of the peaks could be indexed on a rhombohedral α-$NaFeO_2$ structure, viz., $LiNi_{0.5}Mn_{0.5}O_2$ with $R\bar{3}m$ space group (JCPDS No.: 01-088-0657), few other significant peaks show striking similarity with that of the monoclinic Li_2SnO_3 phase, according to JCPDS No.: 31-0761. The lattice parameter values of $LiNi_{0.5}Mn_{0.5}O_2$, calculated from the unit cell software as a = 2.881 Å, c = 14.278 Å, and the unit cell volume of 102.61 Å^3, are consistent with literature values.[11,12] It is well-known that the mobile lithium ions occupy the octahedral sites of one layer,

DOI: 10.1021/acs.inorgchem.5b01246
Inorg. Chem. 2015, 54, 8590−8597

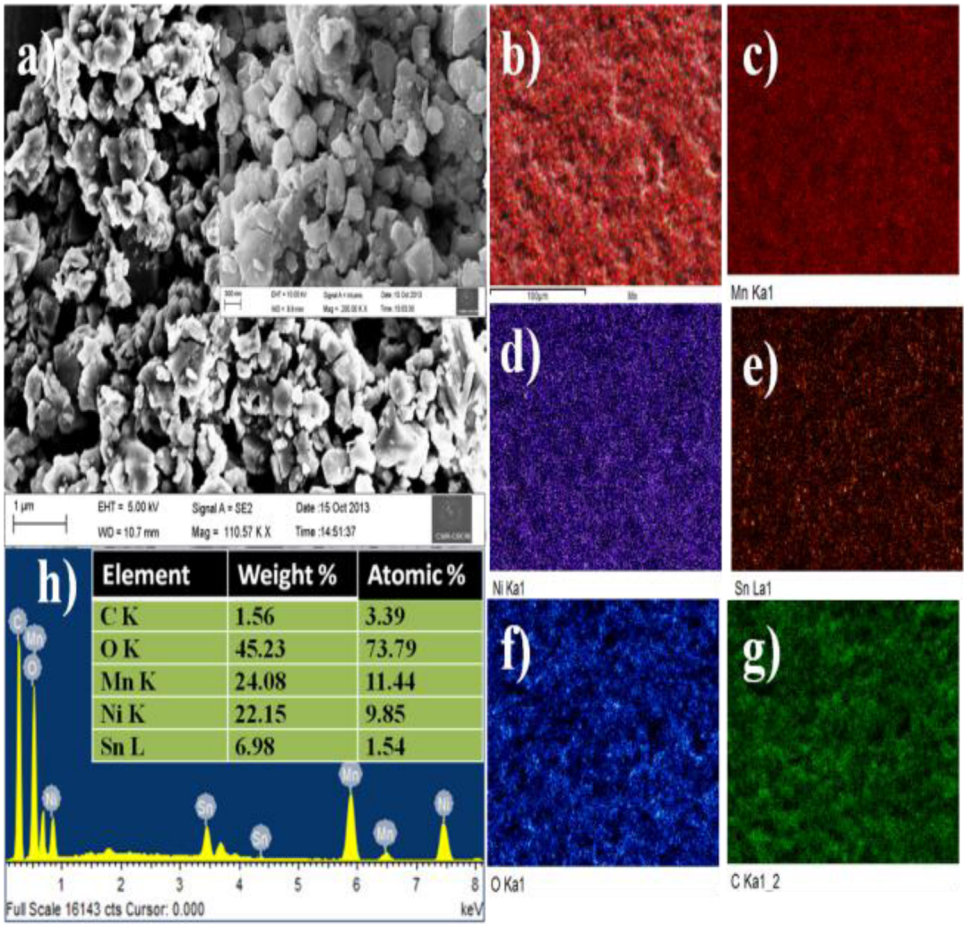

Figure 2. (a) FESEM image of pristine $Li_2Mn_{0.5}Ni_{0.5}SnO_4$. Inset: closer view of morphology. (b) Cumulative and (c–g) individual elemental mapping analysis and (h) EDS results of $Li_2Mn_{0.5}Ni_{0.5}SnO_4$/C composite.

while the nickel and manganese atoms fill the octahedral positions of adjacent layers to form the ordered layered structured with hexagonally close packed oxygen atoms.

Accordingly, the distinct separation of (006) from (102) and (108) from (110) peaks substantiates the formation of rhombohedral phase with highly ordered layered structure. Particularly, the XRD pattern shows a less intense peak at 18.3° (2θ), thereby indicating the presence of Li_2SnO_3 that could be indexed to the monoclinic crystal structure of $C2/c$ space group (JCPDS No.: 31-0761). The lattice parameter values of Li_2SnO_3 have been calculated as a = 5.3012, b = 9.1710, and c = 10.0170 using the unit cell software. Based on these grounds, it is believed that $Li_2Ni_{0.5}Mn_{0.5}SnO_4$ exists as a hybrid containing $LiNi_{0.5}Mn_{0.5}O_2$ and Li_2SnO_3, as mentioned earlier. Unlike Li_2MnSnO_4 (studied by the same group) that exists as a single phase compound when prepared as pristine product and leads to the formation of a hybrid consisting of Mn_2SnO_4 and Li_2SnO_3 especially when prepared in the form of a composite, the currently aimed $Li_2Ni_{0.5}Mn_{0.5}SnO_4$ compound exists as a hybrid consisting of layered $LiNi_{0.5}Mn_{0.5}O_2$ and monoclinic Li_2SnO_3, irrespective of its preparation as pristine or as composite. Hence it is understood that the partial replacement of Mn with Ni offers the inherent advantage of obtaining a desired hybrid composition to realize beneficial electrochemical properties, without requiring the addition of extra carbon. However, considering the poor electronic conductivity of $LiMSnO_4$ family compounds, a minimum concentration of 10 wt % super P carbon has been added to prepare $Li_2Ni_{0.5}Mn_{0.5}SnO_4$/C to qualify the composite as a potential electrode material for lithium battery application. Interestingly, the XRD pattern of $Li_2Ni_{0.5}Mn_{0.5}SnO_4$/C composite shows striking similarity with the pristine $Li_2Ni_{0.5}Mn_{0.5}SnO_4$. Despite the similarity observed in XRD analysis, $Li_2Ni_{0.5}Mn_{0.5}SnO_4$/C composite has been compared with the corresponding pristine product in select characterization studies, with a view to understand the presence and role of carbon in improving the conductivity and the subsequent electrochemical properties, improved as a function of enhanced Li^+ ion diffusion kinetics. FESEM image (Figure 2a) of the currently synthesized $Li_2Ni_{0.5}Mn_{0.5}SnO_4$/C composite consisting of Li_2SnO_3·$LiNi_{0.5}Mn_{0.5}O_2$ hybrid evidences the presence of uneven particles, which are closely connected with each other to form a dense structure. An average particle size of 100–200 nm is seen from the recorded image (inset of Figure 2a).

Elemental mapping (Figure 2b–g) of Li_2SnO_3·$LiNi_{0.5}Mn_{0.5}O_2$/C composite, with a special reference to cumulative elemental mapping (Figure 2b), confirms the presence of uniform distribution of Mn, Ni, Sn, O, and C in the individual particles. Energy dispersive spectroscopy (EDS) analysis of the sample evidences the coexistence of carbon, oxygen, manganese, nickel, and tin, as shown in Figure 2h. The atomic ratio of the aforementioned elements is about 3.39, 73.79, 11.44, 9.85, and 1.54% respectively, as estimated from the EDS result. The total carbon content of the title composite has been calculated using TGA and is found to be 10 wt %

DOI: 10.1021/acs.inorgchem.5b01246
Inorg. Chem. 2015, 54, 8590–8597

(Figure S1), which is in accordance with the externally added carbon to form the $Li_2Ni_{0.5}Mn_{0.5}SnO_4/C$ composite.

The actual particle size and the existence of carbon on the surface of $Li_2SnO_3{\cdot}LiNi_{0.5}Mn_{0.5}O_2$ hybrid composition have been investigated by TEM studies (Figure 3). The correspond-

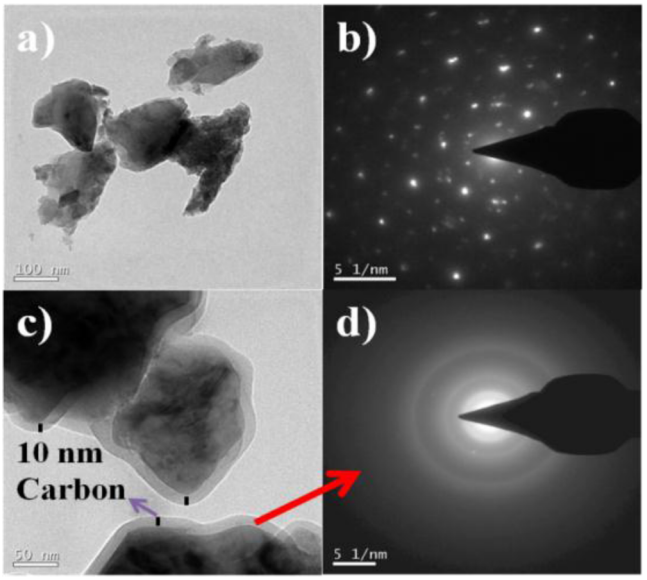

Figure 3. (a) TEM image, (b) SAED pattern of pristine $Li_2Ni_{0.5}Mn_{0.5}SnO_4$, (c) TEM image, and (d) SAED pattern of carbon present in $Li_2Ni_{0.5}Mn_{0.5}SnO_4/C$ composite.

ing SAED pattern is appended as Figure 3b that confirms the polycrystalline nature of the pristine $Li_2SnO_3{\cdot}LiNi_{0.5}Mn_{0.5}O_2$ product obtained from the sol–gel method. The TEM image shows the presence of particles of about 100 nm size (Figure 3a). Further, TEM evidences the presence of carbon coating on $Li_2SnO_3{\cdot}LiNi_{0.5}Mn_{0.5}O_2$ particles (Figure 3c), which is in favor of the fact that the externally added super P carbon acts as a surface modifying coating material. The presence of a conducting carbon network and a desirable coating thickness (10 nm) of carbon coverage are clearly evident from Figure 3c. In addition, the amorphous nature of the added super P carbon (Figure 3d) that forms a thin carbon cloud around the active material is evident from Figure 3c. Further, TEM based individual and cumulative (Figure S2) elemental mapping results of $Li_2Ni_{0.5}Mn_{0.5}SnO_4/C$ evidence the presence of Ni, Mn, Sn, O, and C as components of every individual particle, which is in line with the FESEM results shown in Figure 2.

Subsequently, Figure 4 shows a high resolution TEM (HRTEM) image, wherein the crystal lattice clearly reveals two kinds of lattice fringes with a lattice spacing of about 0.47 and 0.38 nm, which can be assigned to the (003) planes of rhombohedral $LiNi_{0.5}Mn_{0.5}O_2$ nanocrystals and the (111) planes of monoclinic Li_2SnO_3 nanocrystals, respectively. Hence, the coexistence of layered $LiNi_{0.5}Mn_{0.5}O_2$ and the monoclinic Li_2SnO_3 in the hybrid composition of $Li_2Ni_{0.5}Mn_{0.5}SnO_4/C$, as inferred from XRD, has been substantiated from HRTEM analysis.

X-ray photoelectron spectroscopy (XPS) measurements were carried out to confirm the oxidation state of Ni, Mn, O, and Sn. Figure S3 (panels a and b) indicates the 2p spectrum of each transition metal, which splits into two spin–orbit coupling components, namely, $2p_{3/2}$ and $2p_{1/2}$. The $2p_{3/2}$ peaks of Ni and Mn, corresponding to the title compound, occurs at the

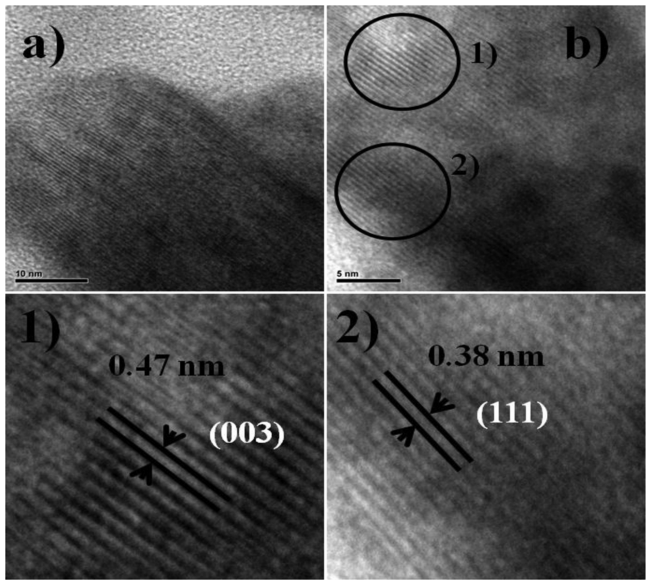

Figure 4. HRTEM image of $Li_2Ni_{0.5}Mn_{0.5}SnO_4/C$ containing $Li_2SnO_3{\cdot}LiNi_{0.5}Mn_{0.5}O_2$ hybrid composition.

binding energy value of 853.8 and 643.2 eV respectively.[13] Further, an O 1s spectrum has a peak at 530.5 eV, thus favoring the 2^+ oxidation[14] state for oxygen in the $Li_2SnO_3{\cdot}LiNi_{0.5}Mn_{0.5}O_2/C$ composite. The Sn 3d spectrum exhibits spin–orbit doublet peaks at 486.7 and 495.4 eV for $3d_{5/2}$ and $3d_{3/2}$ respectively, which in turn matches with the binding energy of Sn(IV).[15,16] Based on these values, the oxidation state of Ni^{2+}, Mn^{4+}, O^{2-}, and Sn^{4+} has been confirmed from XPS analysis. This in turn substantiates the composition of the hybrid, namely, Li_2SnO_3 and $LiNi_{0.5}Mn_{0.5}O_2$, as deduced from XRD results. Brunauer–Emmett–Teller (BET) analysis of $Li_2Ni_{0.5}Mn_{0.5}SnO_4/C$ nanoparticles shows a specific surface area of 48.9 $m^2\ g^{-1}$ with a pore volume of 0.137 $cm^3\ g^{-1}$ (Figure S4).

Figure 5a shows typical cyclic voltammogram (CV) of $Li_2Ni_{0.5}Mn_{0.5}SnO_4/C$ consisting of Li_2SnO_3 and $LiNi_{0.5}Mn_{0.5}O_2$ components in the composite electrode. CV is recorded in the potential window between 3.5 and 0.01 V and at a scan rate of 0.05 mV s^{-1}. Several reduction and oxidation peaks could be observed in the CV results, implying that the sample undergoes multiple redox mechanism. Upon discharge, one among the hybrid components of the title compound, viz., $LiNi_{0.5}Mn_{0.5}O_2$, undergoes direct lithiation to form dilithium layered oxide, according to the following equation:[10]

$$LiNi_{0.5}Mn_{0.5}O_2 + Li \rightarrow Li_2Ni_{0.5}Mn_{0.5}O_2 \quad (2)$$

Herein, the Mn^{4+} ions are reduced to Mn^{2+} ions to form $Li_2Mn_{0.5}Ni_{0.5}O_2$, which is incidentally a mid member of solid solutions ranging from Li_2MnO_2 and Li_2NiO_2.[17−19] The formed $Li_2Ni_{0.5}Mn_{0.5}O_2$ further undergoes a displacement reaction to form Ni and MnO as per eq 3:[11]

$$Li_2Ni_{0.5}Mn_{0.5}O_2 + Li^+ \rightarrow 1.5Li_2O + 0.5Ni + 0.5MnO \quad (3)$$

Simultaneously, the other component of the hybrid composition, viz., Li_2SnO_3, also undergoes decomposition reaction to form SnO_2 and Li_2O, according to eq 4.[8]

$$Li_2SnO_3 \rightarrow SnO_2 + Li_2O \quad (4)$$

DOI: 10.1021/acs.inorgchem.5b01246
Inorg. Chem. 2015, 54, 8590−8597

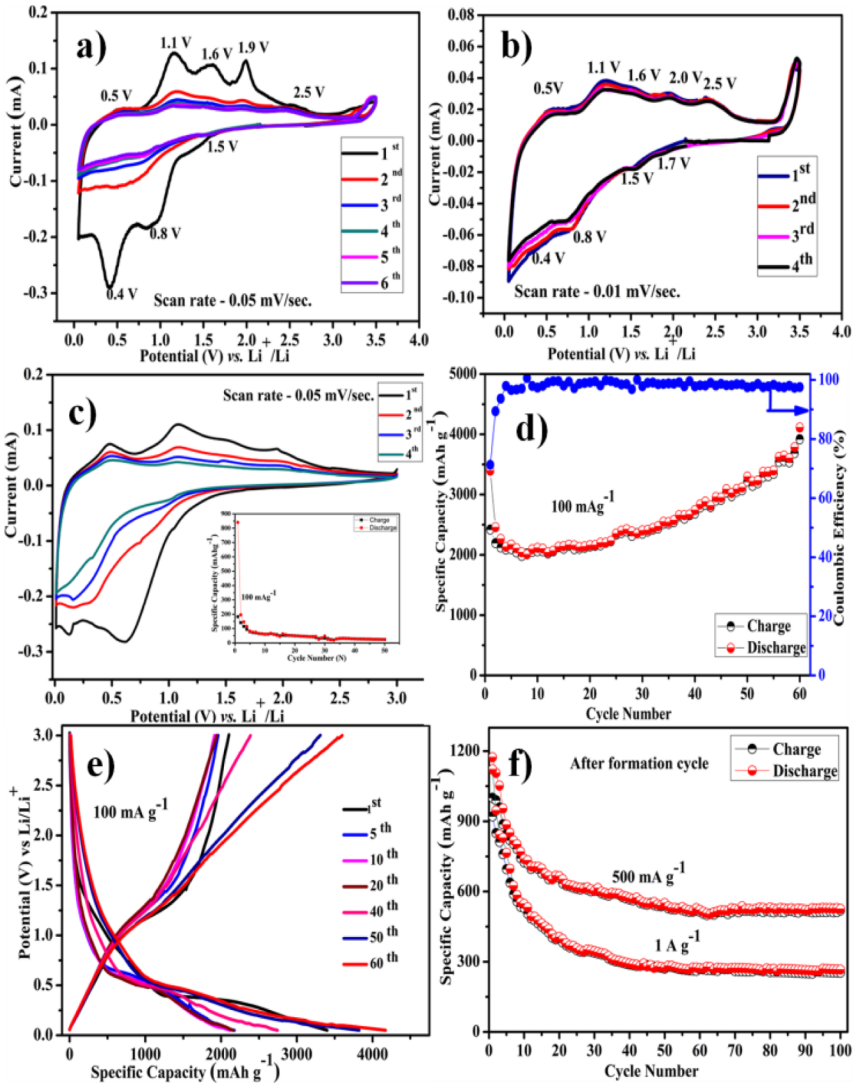

Figure 5. (a) Cyclic voltammogram of $Li_2Ni_{0.5}Mn_{0.5}SnO_4/C$ composite anode recorded at a scan rate of 0.05 mV s^{-1}. (b) CV behavior at a scan rate of 0.01 mV s^{-1}. (C) Cyclic voltammogram of pristine $Li_2Ni_{0.5}Mn_{0.5}SnO_4$ anode recorded at scan rate of 0.05 mV s^{-1}; (inset) cycling behavior of pristine $Li_2Ni_{0.5}Mn_{0.5}SnO_4$ anode at 100 mA g^{-1} current density. (d) Extended cycling behavior of $Li_2Ni_{0.5}Mn_{0.5}SnO_4/C$ anode up to 60 cycles (100 mA g^{-1}). (e) Capacity vs voltage profile of $Li_2Ni_{0.5}Mn_{0.5}SnO_4/C$ anode. (f) Extended cyclability of $Li_2Ni_{0.5}Mn_{0.5}SnO_4/C$ anode at 500 and 1000 mA g^{-1} current density.

Interestingly, the currently recordered CV (Figure 5a) exhibits a reduction peak at 1.7 V due to the formation of dilithium oxide (obviously seen from Figure 5b), viz., $Li_2Ni_{0.5}Mn_{0.5}O_2$, another peak at 1.5 V corresponding to the formation of Mn^0, and a third peak at 0.8 V due to Ni^0 and Sn^0 during the course of the discharge process.[8,20] Similarly, the structural decomposition of SnO_2 (obtained from Li_2SnO_3) leads to the formation of Li_2O, according to a partially irreversible reaction such as[8]

$$SnO_2 + xLi^+ + xe^- \rightarrow Sn^0 + 2Li_2O \quad (5)$$

Subsequently, Sn thus formed is involved in the alloying reaction with lithium at 0.4 V to form $Li_{4.4}Sn$ in a reversible manner, according to eq 6[21]

$$Sn^0 + xLi^+ + xe^- \leftrightarrow Li_xSn \quad \text{where} \quad 0 \le x \le 4.4 \quad (6)$$

Upon charge, the in situ formed $Li_{4.4}Sn$ alloy undergoes a dealloying reaction at 0.55 V and further oxidation to form SnO at 1.1 V.[22] The formed SnO upon further oxidation forms SnO_2 at 1.6 V.[22] Subsequently, oxidation of Ni and Mn to form the respective oxides takes place at 2.0 and 2.5 V, according to eqs 7 and 8:[8,20]

$$Ni + Li_2O \leftrightarrow 2Li^+ + NiO + 2e^- \quad (7)$$

$$Mn + Li_2O \leftrightarrow 2Li^+ + MnO + 2e^- \quad (8)$$

Hence, the cyclic reversibility of $Li_2Ni_{0.5}Mn_{0.5}SnO_4/C$ anode could be understood in terms of lithiation and delithiation of components present in the hybrid composition, viz., $LiNi_{0.5}Mn_{0.5}O_2$ and Li_2SnO_3. It is noteworthy to mention here that the cyclic reversibility is excellent for the $Li_2Ni_{0.5}Mn_{0.5}SnO_4/C$ anode, wherein no significant difference in CV pattern has been noticed upon progressive cycling, especially when cycled at a slow scan rate of 0.01 mV s^{-1} (Figure 5b). This is an indication that the $Li_2Ni_{0.5}Mn_{0.5}SnO_4/C$ anode would exhibit better electrochemical performance than the pristine $Li_2Ni_{0.5}Mn_{0.5}SnO_4$ anode, based on known reasons of increased electronic conductivity and also in accordance with the inference derived from the physical characterization studies.

DOI: 10.1021/acs.inorgchem.5b01246
Inorg. Chem. 2015, 54, 8590−8597

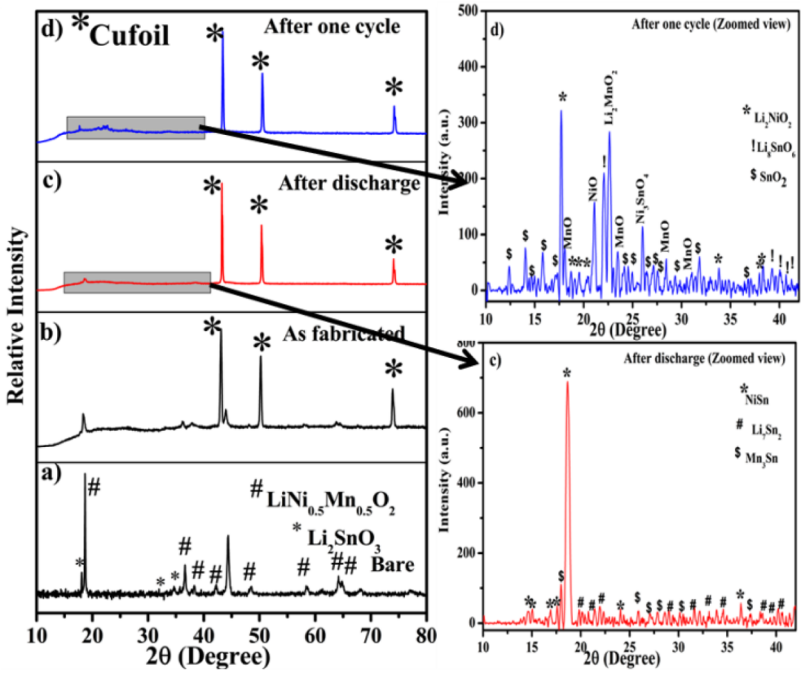

Figure 6. Ex situ XRD study of (a) pristine $Li_2Ni_{0.5}Mn_{0.5}SnO_4$ compound, (b) $Li_2Ni_{0.5}Mn_{0.5}SnO_4$/C coated on a Cu foil (recovered from the as fabricated cell), (c) $Li_2Ni_{0.5}Mn_{0.5}SnO_4$/C recovered after discharge to 0.01 V, and (d) $Li_2Ni_{0.5}Mn_{0.5}SnO_4$/C anode after the completion of one cycle.

The larger difference in the CV pattern (upon cycling) observed with the pristine $Li_2Ni_{0.5}Mn_{0.5}SnO_4$ anode (Figure 5c) could be better understood and substantiated from the inferior charge−discharge behavior exhibited by the same (inset of Figure 5c). In other words, pristine $Li_2Ni_{0.5}Mn_{0.5}SnO_4$ anode exhibits a capacity as low as 25 mAh g^{-1} at the 50th cycle, at 100 mA g^{-1} current density. Galvanostatic discharge−charge cycling was carried out with $Li_2Ni_{0.5}Mn_{0.5}SnO_4$/C in the voltage range from 0.01 to 3.0 V, under a current density of 100 mA g^{-1} (Figure 5d). An appreciable initial discharge capacity of 3382 mAh g^{-1} and a corresponding charge capacity of 2380 mAh g^{-1} with a Coulombic efficiency of 70.3% have been exhibited by $Li_2Ni_{0.5}Mn_{0.5}SnO_4$/C composite anode. The observed initial irreversible capacity loss of 27.6% may be attributed to the irreversible process that involves the tapping of fraction of lithium from the electrode material. In other words, the observed capacity loss in the first cycle is attributed to the initial irreversible loss of lithium during the formation of a solid electrolyte interface (SEI) and electrolyte decomposition, which are common for lithium intercalating electrode materials.[8,23,24] More interestingly, the progressive capacity is found to increase gradually after 10 cycles, and when the cycling exceeds 50 cycles, an increased discharge capacity of 3830 mAh g^{-1} and a charge capacity of 3750 mAh g^{-1} have been observed with the substantially increased Coulombic efficiency of 98%, which is the highlight of the study.

Reasons for the gradually increasing capacity behavior upon extended cycling involve (a) reversibility of several redox reactions (discussed in CV), (b) probable formation and reversible decomposition of polymeric/gel like layer facilitated by the initial decomposition of the electrolyte that offers better adherence apart from the provision of enhanced cohesion to encourage extra lithium storage sites and protection against parasitic side reactions,[25−27] and (c) partial reversibility[8,20] of $SnO_2 + xLi^+ + xe^- \rightarrow Sn^0 + 2Li_2O$ reaction upon cycling (as evidenced by the concurrent appearance of the CV peak at 1.1 V upon progressive cycling). Such an increasing capacity contribution observed upon extended cycle life is reported to be common for Sn based electrodes and SnO_2/graphene nanocomposite,[26,28] Sn/C nanocomposite,[29] Si/C nanocomposite,[30] and other metal oxide systems,[31,32] especially when exploited as anodes. Figure 5e shows the charge−discharge profile of the $Li_2Ni_{0.5}Mn_{0.5}SnO_4$/C composite anode recorded under a current density of 100 mA g^{-1} between 0.01 and 3.0 V. The appreciable initial discharge capacity of 3382 mAh g^{-1} and a corresponding charge capacity of 2380 mAh g^{-1}, followed by 2755 and 2394 mA h g^{-1} at the 40th cycle, 3830 and 3750 mAh g^{-1} at the 50th cycle, and 4104 and 4000 mA h g^{-1} at the 60th cycle, have been observed, as evident from Figure 5e.

The electrochemical stability of synthesized $Li_2Ni_{0.5}Mn_{0.5}SnO_4$/C composite anode upon extended cycling could be better understood from the appended charge−discharge profile pattern (Figure 5e). Further, the suitability of the title anode for extended cycle life, especially under the influence of moderate and high current density of 500 and 1000 mA g^{-1} up to 100 cycles, has been investigated (Figure 5f). Despite the extremely higher initial discharge capacity values of 1178 and 1100 mAh g^{-1} observed at 500 mA g^{-1} and 1000 mA g^{-1} respectively, an average progressive capacity of ∼600 and 300 mAh g^{-1} has been exhibited by $Li_2Ni_{0.5}Mn_{0.5}SnO_4$/C anode. Particularly at the end of the 100th cycle, the composite anode delivers a capacity of around 500 and 300 mA h g^{-1} respectively under the influence of 500 and 1000 mA g^{-1} current density, thus demonstrating its suitability for high rate applications.

With a view to understand and to investigate upon the cycling stability of title composite electrode, which is believed to undergo a series of lithiation/delithiation, displacement/conversion, and alloying/dealloying reaction mechanism, ex situ XRD study has been attempted with the as prepared powder, as fabricated electrode, and electrode after completing one discharge and one cycle individually (Figure 6). Figure 6a

DOI: 10.1021/acs.inorgchem.5b01246
Inorg. Chem. 2015, 54, 8590−8597

evidences the coexistence of Li_2SnO_3 and $LiNi_{0.5}Mn_{0.5}O_2$ present in $Li_2Ni_{0.5}Mn_{0.5}SnO_4$, and Figure 6b depicts the peak pattern observed for the corresponding composite coated on Cu foil, wherein peaks dominant due to Cu are indicated with the * mark. Upon discharge (lithiation), the newly formed $Li_2Ni_{0.5}Mn_{0.5}O_2$ and the corresponding formation of Li_2O, Ni, and MnO (according to eqs 2 and 3) along with the displacement reaction originated products of Li_2SnO_3 (eq 4) cumulatively lead to the existence of amorphous phases of Li_7Sn_2, NiSn, and Mn_3Sn alloys, which are evident from the zoomed peak pattern, furnished against Figure 6c. Similarly the reversibly formed crystalline products, according to equations such as $Li_8SnO_6 \rightarrow 4Li_2O + SnO_2$, $Li_2NiO_2 \rightarrow Li_2O + NiO$, and $Li_2MnO_2 \rightarrow Li_2O + MnO$, due to dealloying and conversion reactions, are obvious from the zoomed view of Figure 6d. Hence, the structural stability of the title electrode upon progressive cycling aided by the reversibly formed products is substantiated from the ex situ XRD studies.

Subsequently, the title composite electrode has been subjected to rate capability test, wherein noticeable specific capacity values of 650, 600, 510, and 450 mAh g^{-1} have been observed after 10, 20, 30, and 40 cycles corresponding to the current density values of 600, 700, 800, and 900 mA g^{-1} (Figure 7).

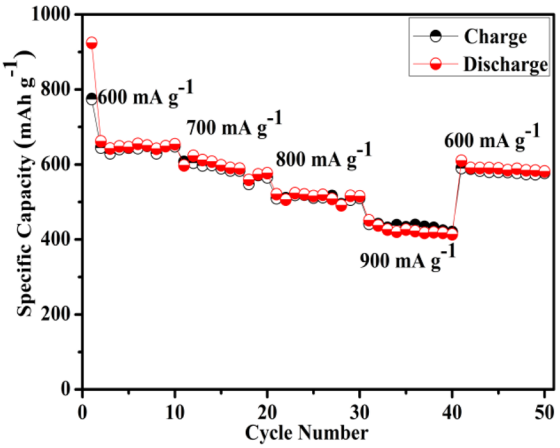

Figure 7. Rate capability of $Li_2Mn_{0.5}Ni_{0.5}SnO_4$/C anode.

Interestingly, $Li_2Ni_{0.5}Mn_{0.5}SnO_4$/C composite anode, even after being subjected to a high current density of 900 mA g^{-1}, is capable of exhibiting an acceptable capacity of 590 mAh g^{-1}, especially when brought back to the initial discharge condition of 600 mA g^{-1}, which is an indication of better retention of capacity. Hence, the versatile suitability of currently synthesized $Li_2Ni_{0.5}Mn_{0.5}SnO_4$/C composite electrode for high rate lithium battery applications has been demonstrated.

Electrochemical impedance (EIS) spectroscopy was performed on a Biologic VMP3 multichannel potentiostat to understand the Li^+ ion transfer behavior in pristine $Li_2Ni_{0.5}Mn_{0.5}SnO_4$ and $Li_2Ni_{0.5}Mn_{0.5}SnO_4$/C composite electrodes. The Nyquist plots are recorded potentiostatically by applying an ac voltage of 5 mV amplitude in the 100 kHz to 10 mHz frequency range. Figure 8 shows the results of EIS analysis (fitted with an equivalent circuit model) of $Li_2Ni_{0.5}Mn_{0.5}SnO_4$ and $Li_2Ni_{0.5}Mn_{0.5}SnO_4$/C composite electrodes (charged to 3.0 V vs Li^+/Li) after 20 cycles, and the normalized EIS spectrum is appended as an inset. The observed R_{ct} values of bare $Li_2Mn_{0.5}Ni_{0.5}SnO_4$ and $Li_2Ni_{0.5}Mn_{0.5}SnO_4$/C composite are

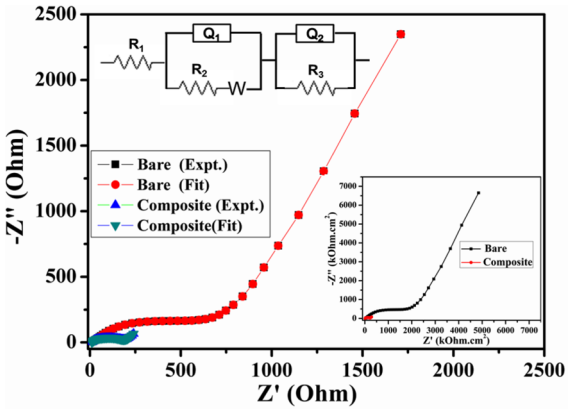

Figure 8. Impedance plots of pristine and $Li_2Mn_{0.5}Ni_{0.5}SnO_4$/C anodes. Inset: Normalized EIS spectrum.

724 and 180 Ω respectively (Figure 8). The corresponding normalized R_{ct} values pertinent to $Li_2Ni_{0.5}Mn_{0.5}SnO_4$ and $Li_2Ni_{0.5}Mn_{0.5}SnO_4$/C are 1810 and 223 kΩ·$cm^2$ respectively (inset of Figure 8). It is evident from Figure 8 that the semicircle arc of $Li_2Ni_{0.5}Mn_{0.5}SnO_4$/C composite is smaller than that of pristine $Li_2Ni_{0.5}Mn_{0.5}SnO_4$ anode after 20 cycles, which is an indication of reduced internal resistance and the subsequently improved electronic conductivity, as a function of carbon coating. Hence, the currently observed EIS behavior of $Li_2Ni_{0.5}Mn_{0.5}SnO_4$/C composite anode substantiates the advantages of carbon coating in improving the cycling performance of pristine $Li_2Ni_{0.5}Mn_{0.5}SnO_4$ anode.

4. CONCLUSIONS

Exploration of newer formulation of $Li_2Ni_{0.5}Mn_{0.5}SnO_4$/C composite electrode for high capacity and high rate lithium battery applications has been demonstrated with excellent electrochemical behavior. More interestingly, the synergistic contribution of counterparts of the hybrid, viz., Li_2SnO_3 and $LiNi_{0.5}Mn_{0.5}O_2$, in realizing the potential electrochemical behavior of $Li_2Ni_{0.5}Mn_{0.5}SnO_4$ anode assumes importance. While the composition of the hybrid attributes to the anode behavior, the added carbon to form $Li_2Ni_{0.5}Mn_{0.5}SnO_4$/C anode plays a significant role in qualifying the title anode for its high and rated capacity behavior. A combination of alloying/dealloying, displacement, and conversion reaction mechanism related to Li_2SnO_3 and Ni/Mn components of $Li_2Ni_{0.5}Mn_{0.5}O_2$ derived from $LiNi_{0.5}Mn_{0.5}O_2$ amounts to the observed capacity of >3000 mAh g^{-1} at 100 mA g^{-1} even after completing 50 cycles. More interestingly, the anode exhibits a capacity of ~300 mAh g^{-1} at 1 A g^{-1} current density, thus qualifying itself as a rated capacity anode material. The observed high capacity (600 mAh g^{-1} at 500 mA g^{-1}) and rated capacity (300 mAh g^{-1} at 1 A g^{-1}) behavior of $Li_2Ni_{0.5}Mn_{0.5}SnO_4$/C composite anode up to 100 cycles leads to the possible consideration of new class of Li_2SnO_3·$LiM_1M_2O_2$ hybrid composition as yet another potential anode formulation for application in rechargeable lithium batteries.

■ ASSOCIATED CONTENT

Supporting Information

The Supporting Information is available free of charge on the ACS Publications website at DOI: 10.1021/acs.inorgchem.5b01246.

DOI: 10.1021/acs.inorgchem.5b01246
Inorg. Chem. 2015, 54, 8590−8597

TGA, XPS, TEM elemental mapping, and BET analysis (PDF)

AUTHOR INFORMATION

Corresponding Author

*Tel: +91 4565 241427. Fax: +91 4565 227779. E-mail: kalaiselvicecri@gmail.com.

Notes

The authors declare no competing financial interest.

ACKNOWLEDGMENTS

Department of Science and Technology (DST) and CSIR, New Delhi, are acknowledged for financial support respectively through GAP-14/11 and MULTIFUN (CSC-0101) Projects.

REFERENCES

(1) Thackeray, M. M.; Vaughey, J. T.; Kahaian, A. J.; Kepler, K. D.; Benedek, R. *Electrochem. Commun.* **1999**, *1*, 111−115.
(2) Benedek, R.; Thackeray, M. M. *J. Power Sources* **2002**, *110*, 406−411.
(3) Mahmood, N.; Zhang, C.; Liu, F.; Zhu, J.; Hou, Y. *ACS Nano* **2013**, *7*, 10307−10318.
(4) Sharma, N.; Shaju, K. M.; Subba Rao, G. V.; Chowdari, B. V. R. *Electrochem. Commun.* **2002**, *4*, 947−952.
(5) Poizot, P.; Laruelle, S.; Grugeon, S.; Dupont, L.; Tarascon, J.-M. *Nature* **2000**, *407*, 496−499.
(6) Zhang, W. M.; Wu, X. L.; Hu, J. S.; Guo, Y. G.; Wan, L. J. *Adv. Funct. Mater.* **2008**, *18*, 3941−3946.
(7) Wang, D.; Belharouak, I.; Zhang, X.; Ren, Y.; Meng, G.; Wang, C. *J. Electrochem. Soc.* **2014**, *161* (1), A1−A5.
(8) Mani, V.; Babu, G.; Kalaiselvi, N. *Electrochim. Acta* **2014**, *133*, 347−353.
(9) Gao, B.; Kleinhammes, A.; Tang, X. P.; Bower, C.; Fleming, L.; Wu, Y.; Zhou, O. *Chem. Phys. Lett.* **1999**, *307*, 153−157.
(10) Vaughey, J. T.; Geyer, A. M.; Fackler, N.; Johnson, C. S.; Edstrom, K.; Bryngelsson, H.; Benedek, R.; Thackeray, M. M. *J. Power Sources* **2007**, *174*, 1052−1056.
(11) Johnson, C. S.; Kim, J. S.; Kropf, A. J.; Kahaian, A. J.; Vaughey, J. T.; Fransson, L. M. L.; Edstrom, K.; Thackeray, M. M. *Chem. Mater.* **2003**, *15*, 2313.
(12) Jiang, Y.; Yang, Z.; Luo, W.; Hu, X.; Huang, Y. *Phys. Chem. Chem. Phys.* **2013**, *15*, 2954−2322.
(13) Kang, S. H.; Kim, J.; Stoll, M. E.; Abraham, D.; Sun, Y. K.; Amine, K. *J. Power Sources* **2002**, *112*, 41−48.
(14) Zhang, L.; Ge, S.; Zuo, Y.; Zhang, B.; Xi, L. *J. Phys. Chem. C* **2010**, *114*, 7541−7547.
(15) Wang, C.; Du, G.; Stahl, K.; Huang, H.; Zhong, Y.; Jiang, J. Z. *J. Phys. Chem. C* **2012**, *116*, 4000−4011.
(16) Ahn, H. J.; Choi, H. C.; Park, W. K.; Kim, S. B.; Sung, Y. E. *J. Phys. Chem. B* **2004**, *108*, 9815−9820.
(17) David, W. I. F.; Goodenough, J. B.; Thackeray, M. M.; Thomas, J. M. *Rev. Chim. Miner.* **1983**, *20*, 636−642.
(18) Dahn, J. R.; Sacken, U. V.; Michal, C. A. *Solid State Ionics* **1990**, *44*, 87−97.
(19) Johnson, C. S.; Kim, J. S.; Kropf, A. J.; Kahaian, A. J.; Vaughey, J. T.; Thackeray, M. M. *Electrochem. Commun.* **2002**, *4*, 492−498.
(20) Li, X.; Wang, C. *RSC Adv.* **2012**, *2*, 6150−6154.
(21) Xue, M. Z.; Fu, Z. W. *Electrochem. Solid-State Lett.* **2006**, *9*, A468−A470.
(22) Aravindan, V.; Sundaramurthy, J.; Kumar, E. N.; Kumar, P. S.; Ling, W. C.; von Hagen, R.; Mathur, S.; Ramakrishna, S.; Madhavi, S. *Electrochim. Acta* **2014**, *121*, 109−115.
(23) Chen, W.; Ou, Z.; Tang, H.; Wang, H.; Yang, Y. *Electrochim. Acta* **2008**, *53*, 4414−4419.
(24) Lou, X. W.; Deng, D.; Lee, J. Y.; Feng, J.; Archer, L. A. *Adv. Mater.* **2008**, *20*, 258−262.
(25) Zhang, N.; Zhao, Q.; Han, X.; Yang, J.; Chen, J. *Nanoscale* **2014**, *6*, 2827−2832.
(26) Wang, D.; Yang, J.; Li, X.; Geng, D.; Li, R.; Cai, M.; Sham, T.-K.; Sun, X. *Energy Environ. Sci.* **2013**, *6*, 2900−2906.
(27) Wang, D.; Zhao, Y.; Xu, X.; Hercule, K. M.; Yan, M.; An, Q.; Tian, X.; Xu, J.; Qu, L.; Mai, L. *Nanoscale* **2014**, *6*, 8124−8129.
(28) Lian, P.; Zhu, X.; Liang, S.; Li, Z.; Yang, W.; Wang, H. *Electrochim. Acta* **2011**, *56*, 4532−4539.
(29) Xu, Y.; Guo, J.; Wang, C. *J. Mater. Chem.* **2012**, *22*, 9562−9567.
(30) Magasinski, A.; Dixon, P.; Hertzberg, B.; Kvit, A.; Ayala, J.; Yushin, G. *Nat. Mater.* **2010**, *9*, 353−358.
(31) Laruelle, S.; Grugeon, S.; Poizot, P.; Dolle, M.; Dupont, L.; Tarascon, J. M. *J. Electrochem. Soc.* **2002**, *149*, A627−A634.
(32) Xiao, Y.; Wang, X.; Wang, W.; Zhao, D.; Cao, M. *ACS Appl. Mater. Interfaces* **2014**, *6*, 2051−2058.

DOI: 10.1021/acs.inorgchem.5b01246
Inorg. Chem. 2015, 54, 8590−8597